https://doi.org/10.2352/CIC.2022.30.1.15

HDR multispectral imaging-based BRDF measurement using flexible robot arm system

Yoko Arteaga[1] [2] ***, Clotilde Boust***[1] [3]***, Jon Yngve Hardeberg***[2]
[1] ***Centre of Research and Restoration of the Museums of France; Paris, France***
[2] ***Norwegian University of Science and Technology; Gjøvik, Norway***
[3] ***PSL-PCMTH UMR8247 CNRS; Paris, France***

Abstract

Materials with special appearance properties such goniochromatic materials require complex bidirectional measurements to properly characterise their colour and gloss. Normally, these measurements are performed by goniospectrophotometers which are expensive and not commonly available. In this paper a flexible imaging system composed of a snapshot multispectral camera and a light source attached to a robotic arm, is used to obtain HDR BRDF measurements of patinas commonly used in cultural heritage objects. The system is evaluated by comparing the results to those of a commercially available goniospectrophotometer. It is found that with a known uncertainty, the system is capable of producing accurate measurements of samples with a roughness equal or lower than 6.19 µm. For roughnesses higher that 12.48 µm, the accuracy of the system decreases. Moreover, it is found that the size and orientation of the region of interest plays a great influence on the precision of the imaging system.

Introduction

Materials with special appearance properties such as patinas can be called goniochromatic, as their appearance changes at different angles of viewing and illumination. In order to characterise said materials, traditional colour measurements are insufficient [1]. Thus, it is recommended to use devices which perform bidirectional measurements such as goniospectrophotometers. These devices are normally expensive, or the measurements are very time consuming [2].

Patinas are a form of metal polychromy used to decorate metallic artworks in which the colour of the metal is changed. In the field of restoration and conservation, it is important to characterise the appearance of artistic materials and understand how different processes modify it, to carry out better restoration and conservation treatments [3] [4]. Moreover, the proper characterisation of the appearance of said materials is crucial and should be thoroughly studied. Commonly, in museums and conservation workshops, colour and gloss measurements are performed but, these alone are insufficient to provide a complete characterisation of the appearance of complex materials. However, most goniospectrophotometers are not easily available, are expensive and mostly used for the absolute appearance characterisation of materials. Thus the interest in a flexible, cheap, multipurpose system which allows cultural heritage actors to characterise a wide range of materials. Moreover, the accurate capture and modelling of specularities present in materials such as patinas require HDR capture.

In this paper, a flexible HDR multispectral imaging system is used to perform BRDF measurements of bronze patinas commonly found in cultural heritage objects. To evaluate the performance of this system, these measurements are compared to measurements from a commercially available goniospectrophotometer. The flexible HDR multispectral imaging system presented here is composed of a multispectral snapshot camera, and a light source attached to a robotic arm. Due to the flexibility of the robotic-arm, many angles of illumination can be obtained with a very high resolution.

The structure of this paper is as follows: the next section describes the set-up of the imaging system used, the processing pipeline, and the samples studied. The accuracy of this system is evaluated against data obtained from a commercially available goniospectrophotometer and the results are presented in section three, as well as future work. Finally, the conclusion is presented in the fourth section.

Materials and methods

Flexible HDR multispectral-imaging BRDF system

The system presented in this paper is composed of three main elements: a five-joint Dexter robotic arm from Haddington Dynamics [5], a Spectral Filter Array (SFA) multispectral snapshot camera Silios CMS-C [6], and a tilted stage made in-house. This is a modified version of the set-up used in [7].

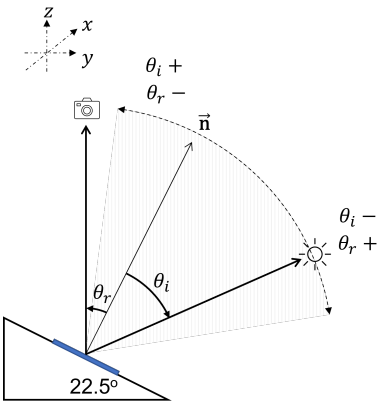

Figure 1: Side view schematic of the system. The camera is looking down on the surface which is on a tilted stage with an elevation of 22.5°. The light is attached to the robotic arm (not illustrated here) and it moves in a 70° arch on the y-z plane.

The robotic arm is used to hold the light source which in this case is a commercially available LED light bulb with a CCT of

6500 K. The robotic arm has the capability of covering a half-hemisphere around the object with an elevation from 10° to 80°. The distance between the light source and the sample is 34 cm. The space available for the movement of the robotic arm is limited due to the shadow cast by the camera at angles close to the viewing angle, and at angles further away from the viewing angle (close to the x-y plane) the light source hits the table. For the purposes of this paper, the sample is illuminated at a fixed angle of observation, $\theta_r = -22.5°$, covering an arch of 35° from both sides of the mirror angle, as illustrated in Figure 1. The angles of illumination range from $\theta_i = -57.5°$ to $\theta_i = 12.5°$, with a total of 63 angles. The illumination sampling is of 3°, 2°, 1°, and 0.5°, increasing as θ_i comes closer to the mirror angle at $\theta_i = -22.5°$. The sampling of the illumination angles is uneven in order to have higher resolution at angles close to the specular peak, and lower at angles further away from it to save processing time and storage.

The multispectral camera used has a 3x3 SFA and it captures eight narrow bands centred at 440nm, 473 nm, 511 nm, 549 nm, 585 nm, 623 nm, 665 nm, and 703 nm. It also has a ninth panchromatic band relatively constant across the visible spectrum. The camera spectral sensitivities are presented in Figure 2. The camera is positioned vertically over the sample at 30 cm, and its optical axis passes through the centre of the arch covered by the robotic arm. The images are acquired at maximum zoom of 3x and maximum aperture size. The effective pixel size is of 0.0377 mm. The samples are placed on an in-house built stage with an angle of elevation of 22.5°. This is chosen so the incident light at the sample ranges equidistantly from the mirror angle. Thus, the angle of observation is of -22.5°. All components of the system are on top of a Thorlabs optical table [8] which removes ambient vibrations.

The robotic arm has five joints which are all controlled from a programming environment. For the given measurement positions, the angles of the joints are calculated using an iterative inverse-kinematic solver. The robotic arm is manually calibrated to its reference position to align it to the virtual 3D kinematic model.

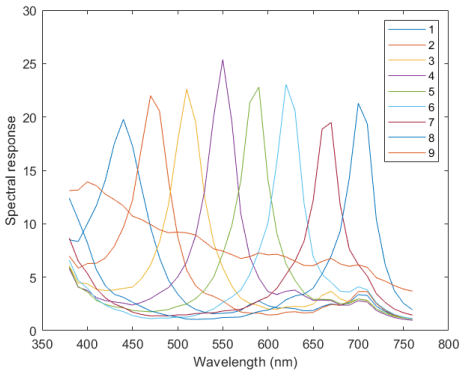

Figure 2: Spectral characteristics of SFA multispectral snapshot camera.

HDR acquisition pipeline

Due to the specularity of the samples, an HDR acquisition pipeline is developed. For each angle of illumination, six images are taken at exposure times 16 ms, 32 ms, 64 ms, 125 ms, 250 ms, and 499 ms. Thus, for 63 angles of illumination, a total of 378 images are taken with an average time of 20 minutes per sample. A cropped area of 660 x 660 pixels (1" x 1") from the centre of the image is stored to reduce the data processing time.

For each acquisition, a dark-current set of images is obtained at the same exposure times to account for dark current in the sensor. The non-uniformity of the light source is also corrected for by performing a flat-field correction. This is done by acquiring a set of images of a uniform white reference target [9].

Data processing pipeline

The data captured by the system is processed to obtain an HDR BRDF of the sample at the chosen viewing angle. The HDR multispectral image is created following the method proposed by Bravers et al. For each sample, at each angle of illumination, six raw images with 10-bit depth are taken with different exposure times. The dark current is subtracted for each exposure time. Each image is linearised using a look-up-table, to obtain values proportional with the object radiance. At this stage, the HDR image is created by performing a weighted average across exposure times, using a modified Tukey window. Due to quantisation effects, camera noise, and saturation noise can be introduced in the image. The weight function thus, favours values in the centre range over those at borders. The weights presented in this paper have been modified from those proposed by Brauers et al. [10] For all exposure times except the shortest (16 ms) and longest (499 ms), values proportional to radiance smaller than 100 and greater than 923 are completely discarded. For the shortest exposure time, the lowest valued pixels are weighted by the Tukey-window. Likewise, for the longest exposure time and highest valued pixels the values are weighted. This is done to keep all relevant information and discard all noise from artefacts such as blooming effect.

A flat-field HDR image of a uniform nearly-Lambertian reference white calibration surface is generated following the same steps to correct for non-uniformity in the illumination. The flat-field correction is performed by multiplying the flat-field image from the HDR image. Then, this HDR radiance map is demosaiced using bilinear interpolation where a multispectral image of 8 bands is obtained as well as a panchromatic image as the ninth channel.

An area of pixels is averaged and spectral reconstruction is performed using the pseudo-inverse method with a regularisation factor, λ=0.0003, to guarantee smooth curves and avoid overfitting. The training data for the reconstruction is a 30 patch colour chart which was measured using the HySpex VNIR-1800 hyperspectral imaging system at 45/0 measurement geometry. Reflectance factors values are interpolated to the range 400 nm - 700 nm in steps of 10 nm.

Evaluation of the system's performance

The BRDF measurement obtained by the system is evaluated against the BRDF of the samples obtained by a commercially available goniospectrophotometer, GON 360, equipped with a CAS 140CT array spectrophotometer [11]. This device provides bidirectional measurements at angles of incidence $\theta_i = -35°, -25°, -15°, -5°, 0°$, and 5°, and angles of reflection θ_r in the range from $-45°$ to 30° in steps of 5°. The measurement spot has a 10 mm diameter. Figure 3 shows the angles measured by the goniospectrophotometer compared to the angles measured by

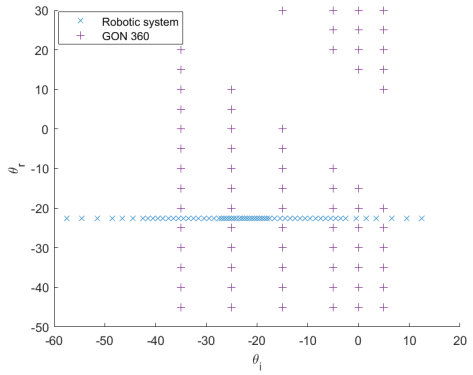

Figure 3: Comparison of both system's measurement range. Blue x markers: robotic arm system. Purple + markers: goniospectrophotometer.

the system as described above.

To evaluate the reflectance factors given by the flexible imaging-based system to the reflectance factors from the goniospectrophotometer, both datasets, $S(\lambda)$ are taken to an independent colour space ie. CIE 1931 XYZ colourspace (Eq. 1) using standard illuminant D65, $I(\lambda)$, and colour matching functions, $\bar{x}(\lambda), \bar{y}(\lambda), \bar{z}(\lambda)$.

$$\begin{bmatrix} X \\ Y \\ Z \end{bmatrix} = \frac{1}{N} \int_{\lambda} S(\lambda) I(\lambda) \begin{bmatrix} \bar{x}(\lambda) \\ \bar{y}(\lambda) \\ \bar{z}(\lambda) \end{bmatrix} d\lambda, \tag{1}$$

where

$$N = \int_{\lambda} I(\lambda) \bar{y}(\lambda) d\lambda. \tag{2}$$

Since the goniospectrophotometer does not measure the samples at the same angles as the system presented in this paper, the values at $\theta_r = -22.5^\circ$ are interpolated using linear interpolation between the measurements at $\theta_r = -20^\circ$ and $\theta_r = -25^\circ$.

Since the system evaluated gives an image-based BRDF, the area and quantity of pixels averaged greatly influences the results. As seen in Figure 1, at the measurement area edges, θ_i and θ_r are changed with respect to those at the middle of the measurement area. Thus, the larger the distance, higher the uncertainty in the measuring angle. Since the distance of the points to the camera changes both θ_i and θ_r, the influence of using different sized averaging windows is studied. The chosen sizes are 100 x 100 pixels, 10 x 10 pixels, 100 x 10 pixels, and 10 x 100 pixels. The averaged areas are presented in Figure 4 and are selected at the centre of the sample.

The rationale behind the choice of windows is that a 100 x 100 pixel averaging window introduces error in the measurement angle, but also it reduces error from averaging the pixel values. Any error introduced from registration issues, problems between acquisitions, or non-uniformity on the sample will be averaged out. Using a 10 x 10 pixel averaging window reduces the error on the angles but consequently, increases the SNR. Also, if the sample is non-uniform, this reduces repeatability, as the results will be highly dependent on the location chosen. A window of 10 x 100 pixels decreases the error induced by the angle, but also maximises the area averaged so the non-uniformity and registration

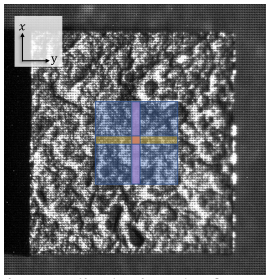

Figure 4: Example image displaying the four averaging windows. In blue 100 x 100, orange 10 x 10, yellow 100 x 10, purple 10 x 100.

errors can be discarded. An area of the same size but in different orientation, 100 x 10 pixels, would increase the error due to the angle uncertainty, but also maximise the area being averaged.

Sample patinas

The samples used for this experiment are bronze patinas from the Coubertin art foundry [12]. Four patinas are available, in two colours: red, and black and two surface finishes: smooth and rough. Hereafter the samples will be referred to as RS, RR, BS, and BR, the first letter being the colour and second their surface finish (smooth or rough). The roughness of the samples, represented by the arithmetical mean height and calculated according to ISO25178 standards [13], is presented in Table 1 [14].

Table 1: Arithmetical mean height (μm) for each patina calculated according to ISO25178 standards. Scanning resolution of 2 μm, using an 8 mm probe.

	Black	Red
Smooth	3.45	6.19
Rough	21.95	12.48

Results and discussion

The calculated luminance, CIE Y, values obtained by the system are plotted as a function of the angle of incidence, θ_i, for the fixed angle of observation, $\theta_r = -22.5^\circ$. For each sample there are four curves corresponding to the four different areas averaged to obtain the CIE Y values. These are displayed as dot markers with error bars. The interpolated values obtained from the goniospectrophotometer are plotted only at the angles of incidence available from the measurements, displayed as black star markers. For the available angles refer to Figure 3.

The standard error of means (SEM) for each point is calculated and displayed as error bars according to:

$$SEM = \frac{\sigma}{\sqrt{N}}, \tag{3}$$

where σ is the standard deviation, and N is the number of observations. The graphs display two standard errors of the mean. Figure 9 shows the mean SEM for each sample and each averaging window.

Smooth samples

Figures 5 and 6, show the curves obtained for the smooth samples. The shape of the curve is smooth and the samples have a peak between $\theta_i = -20°$ and $\theta_i = -25$, close to the theoretical mirror angle at $\theta_i = -22.5°$.

In general, averaging 100 x 100 and 100 x 10 pixels gives a similar response. Averaging 10 x 100 pixels give lower luminance values and a lower specular peak.

BS and RS present similar behaviour. In both cases, the system is precise as the values obtained with the imaging system are quite similar to those from the goniospectrophotometer. The point measured at $\theta_i = -35°$ with the goniospectrophotometer has a slightly higher luminance value than those measured with the imaging system but the shape of the specular peak is well sampled.

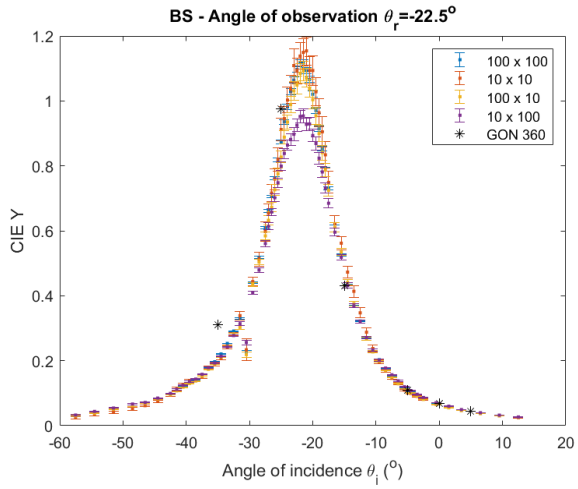

Figure 5: Luminance (CIE Y) as a function of angle of incidence (θ_i) at angle of viewing $\theta_r = -22.5°$. Sample BS.

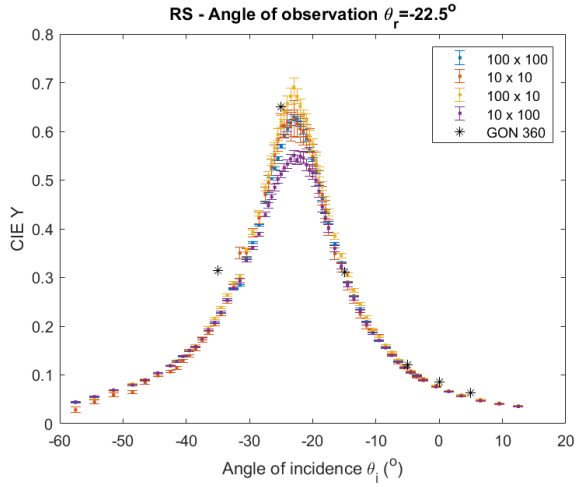

Figure 6: Luminance (CIE Y) as a function of angle of incidence (θ_i) at angle of viewing $\theta_r = -22.5°$. Sample RS.

Rough samples

The rough samples are presented in Figures7, and 8. These samples present quite a different behaviour than that of the smooth

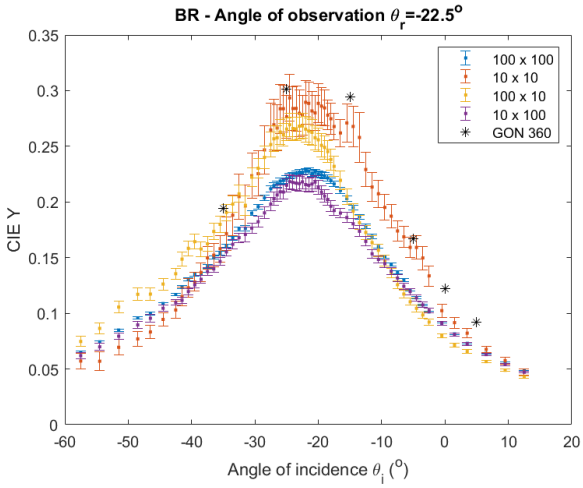

Figure 7: Luminance (CIE Y) as a function of angle of incidence (θ_i) at angle of viewing $\theta_r = -22.5°$. Sample BR.

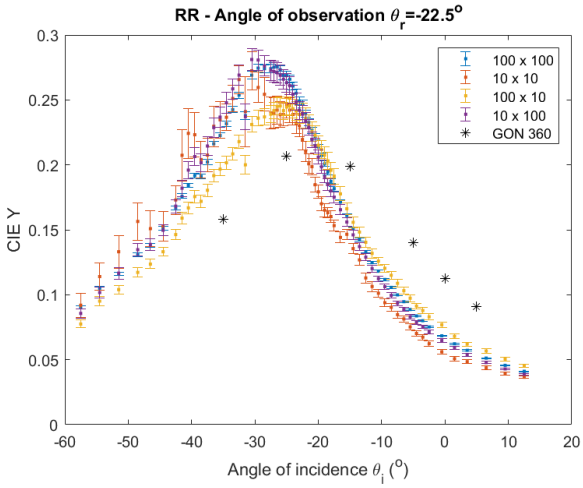

Figure 8: Luminance (CIE Y) as a function of angle of incidence (θ_i) at angle of viewing $\theta_r = -22.5°$. Sample RR.

samples. For BR, the best results are obtained using the 10 x 10 averaging window as they are quite consistent with those from the goniospectrophotometer. However, the 10 x 10 curve is much noisier than the other three. Curves at 100 x 100 and 10 x 100 averaging window have the poorest precision but higher accuracy. The effect of the averaging window is different for RR, presented in Figure 8. All averaging windows give a rather similar curve, with the exception that using 100 x 10 gives a lower specular peak. The main difference between these curves and the ones from the other samples is that the specular peak seems to be shifted to the left, lying between $\theta_i = -25°$ and $\theta_i = -30°$. This could be explained due to the fact the samples are very rough and thus the distribution of microfacets normals could be quite different from the surface normal. Moreover, for sample RR, the curves are quite noisy, particularly 10 x 10, at angles of incidence lower than $\theta_i = -25°$. This could be due to the roughness of the sample and irregularity of the surface. It is possible that many microfacets in the 10 x 10 area are facing the light source at angles smaller than $\theta_i = -25°$, since larger averaging areas have smaller error bars for the same angles.

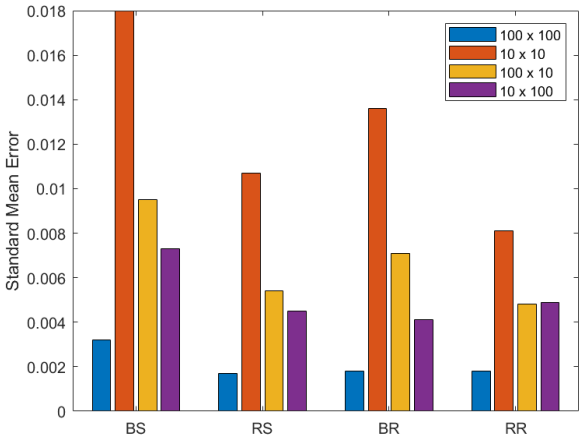

Figure 9: Mean SEM for all samples at different averaged areas.

Precision evaluation

Figure 9 shows the mean of the SEM for all the samples acquired by the custom system, at the four different averaging windows which are presented in Figure 4. Regardless of whether the BRDF curve is accurate or not, the precision of the measurement greatly increases when averaging 100 x 100 pixels. Likewise, averaging 10 x 10 pixels increases the error by almost a full order of magnitude in the case of BS and BR.

In the case of areas 100 x 10 and 10 x 100 which have the same size but different orientation, averaging 10 x 100 reduces the error. As expected and explained before, averaging 10 x 100 pixels minimises the error in both angle of incidence and viewing. Contrary to averaging 100 x 10 pixels which increases the error.

For sample RR, averaging 100 x 10 or 10 x 100 pixels does not change the mean SEM. This could be because this sample is very rough and thus the effect of the non-uniformity of the surface is more significant than the error on the angle.

Discussion and future work

For smooth samples in Figures 5 and 6, it can be seen that the imaging system is as accurate as the goniospectrophotometer. In both cases there is a small difference between the curves obtained by the system presented here and the commercially available goniospectrophotometer. Moreover, the size and orientation does not influence too much the shape of the curves. This suggests the samples are quite uniform as their microfacets normals are oriented evenly which is confirmed by their roughness presented in Table 1. In the case of rough samples, presented in Figures 7 and 8, the system has a lower accuracy at characterising their BRDF than the goniospectrophotometer. In the case of BR, Figure 7, the curve averaging 10 x 10 pixels is accurate as the points measured by the goniospectrophotometer have similar values and the shape of the curves is similar. However the precision at 10 x 10 is rather low. Since both devices work by averaging a small area of the sample, the match in BR could just be a coincidence. If the system was appropriate for this sample, averaging more pixels would increase its accuracy, not decrease it as is the case here. Since this sample has a rough surface, in this case averaging more pixels is equivalent to having a more uneven distribution of microfacets normals. Hence the specular peak at 100 x 100 and 10 x 100 pixels is lower than that at 10 x 10 pixels. In the case of sample RR in Figure 8, the curves do not match the values obtained by the goniospectrophotometer. As it is seen in the graph, the specular peak is at around $\theta_r = -30°$. Moreover, the curves become very noisy at angles lower than the specular peak. This could be also be explained by an averaging effect. This sample is also rough, and it is possible that the area being averaged here has a distribution of microfacets normals which is strongly tilted compared to the area measured by the gioniospectrophotometer. Moreover, it can be seen that the curve obtained by averaging 100 x 10 pixels has a less prominent shift which could indicate the microfacets with a normal shift are lying along the y-axis rather than the x-axis. It must also be noted that the values obtained by the goniospectrophotometer also come from averaging a small area on the sample and that this device is not optimised for samples with this level of roughness.

As mentioned previously, the size and orientation of the averaging area plays a large role in the precision of the system as presented in Figure 9. Regardless of the accuracy of the system and whether the values obtained are confirmed or not by the goniospectrophotometer, averaging a large area decreases the error of the measurement compared to a smaller area. Even if the small area decreases the uncertainty introduced by the viewing and incident angles, the overall error increases. Moreover, equally sized areas at different orientations do not introduce equivalent errors. As mentioned before, averaging 10 x 100 pixels reduces the error because it decreases the uncertainty introduced by the angles of incidence and viewing. The uncertainty in the angle has a strong contribution in the overall precision of the system. However, for sample RR, the error from 100 x 10 is equal to that of 10 x 100. This could be caused by the uncertainty introduced by the non-uniformity of the sample being larger than the contribution from the angle uncertainty.

Given that different points on the sample image give different combinations of incident and viewing angles, this could be used as an advantage. By doing simple trigonometry, it is possible to find the exact angles of incidence and viewing at different points of the sample along the y-axis. Thus, by averaging different equally sized areas along the y-axis, more BRDF measurements can be obtained from a single acquisition, without the need of moving either the camera or the sample. Moreover, since the light source is held by the robotic arm, this provides a lot of flexibility to chose different angles of illumination which can be changed depending on the material being measured. Also, the system presented here has the samples on an in-house built tilted stage. If this stage was replaced by a very accurate, tiltable stage, a further degree of freedom would be introduced which consequently would provide a higher combination of viewing and illumination angles. Finally, it must be noted that this experiment can be repeated with more simple equipment, by replacing the robotic arm by an arch with fixed light sources or a dome type of illumination system which is commonly used in the cultural heritage field for RTI acquisition.

Conclusion

In this paper, a flexible multispectral imaging system and the processing pipeline required to obtain HDR BRDF measurements with it have been presented. The imaging system is used to measure four patina samples commonly used in artistic workshops. The results obtained by the imaging system are compared

to measurements from a commercially available goniospectrophotometer. It is found that for smooth samples with roughness equal or lower than 6.19 μm, the results are reliable as they have a known uncertainty and are consistent with those from the goniospectrophotometer. However, for rough samples with a roughness equal or higher than 12.48 μm, the results present a higher error and the accuracy of the system decreases compare to that of the goniospectrophotometer. For both cases, it is also found that the size and orientation of the averaging window used greatly influences the precision of the imaging system and it should be preferable to use larger areas. Moreover, it is found that the error introduced by the angle uncertainty is higher than that of the non-uniformity of the sample. Finally, it is noteworthy that the illumination system presented here can be easily replaced by simpler and more accessible set-ups such as RTI domes to illuminate the surface at different angles of incidence.

Acknowledgements

This research was funded with the support of CHANGE Cultural Heritage Analysis for New Generations European Union's Horizon 2020 research and innovation programme under the Marie Skłodowska-Curie grant agreement No. 813789.

The authors would like to thank Dominique Robcis for access to the bronze patinas used in this experiment. Many thanks to Tanzima Habib and Donatela Saric for their help measuring the patinas at FOGRA and Vlado Kitanovski for invaluable help with the data acquisition using the robot system.

References

[1] C. McCamy, "Observation and measurement of the appearance of metallic materials. part i. macro appearance", Color Research & Application, 32, p. 378-387, (2007).

[2] A. Sole, I. Farup and P. Nussbaum, "Evaluating an image-based bidirectional reflectance distribution function measurement setup", Applied Optics, 57, p. 1918-1928, (2018).

[3] F. Mathis, S. Descamps, D. Robcis and M. Aucouturier, "Original surface treatment of copper alloy in ancient Roman Empire: chemical patination on a Roman strigil", Surface Engineering, 21, p. 346-351, (2005).

[4] E. Joseph, A. Simon, S. Prati, M. Worle, D. Job and R. Mazzeo, "Development of an analytical procedure for evaluation of the protective behaviour of innovative fungal patinas on archaeological and artistic metal artefacts", Analytical and Bioanalitical Chemistry, 9, (2011).

[5] Haddington Dynamics, online. `https://www.hdrobotic.com`

[6] Silios multispectral cameras, online. `https://silios.com/cms-series`

[7] V. Kitanovski and J. Y. Hardeberg, "Objective evaluation of relighting models on translucent materials from multispectral RTI images", IS&T International Symposium on Electronic Imaging, Material Appearance Conference Proceedings, p. 133-1–133-7, (2021).

[8] Optical breadboards, online. `https://www.thorlabs.com/newgrouppage9.cfm?objectgroup_id=7159`

[9] ColorChecker white balance, online. `https://www.xrite.com/en/categories/calibration-profiling/colorchecker-white-balance`

[10] J. Brauers, N. Schulte, A. A. Bell and T. Aach, "Multispectral High Dynamic Range Imaging", IS&T/SPIE Electronic Imaging, Conference Proceedings, p. 33-42, (2008).

[11] CAS 140CT Array Spectrometer, Instrument Systems. Konica Minolta, online. `https://www.instrumentsystems.com/fileadmin/Downloads/Brochures_Datasheets/CAS140CT_EN.pdf`

[12] J. Edelson, "Elaboration d'une méthodologie d'analyse des patines artificielles sur les bronzes du patrimoine artistique", Master's thesis - École des Mines de Paris (2000).

[13] ISO25178-2:2012 Geometrical product specifications (GPS) - Surface texture: Areal - Part, 2: Terms, definitions and surface texture parameters.

[14] Y. Arteaga, C. Boust, A. Dequier and J. Y. Hardeberg, "Image-based goniometric appearance characterisation of bronze patinas", IS&T Color and Imaging Conference Proceedings, p. 294-299, (2021).

Author Biography

Yoko Arteaga is a Marie Skłodowska-Curie early stage research fellow at the Centre of Research and Restoration of the Museums of France and part of the Colourlab at the Norwegian University of Science and Technology. She has a background in Physics and Colour Science. For her PhD she is working in the development of techniques to characterise surface topography and appearance for cultural heritage objects.

Clotilde Boust is the head of the Imaging Group at the Centre for Research and Restoration of the Museums of France (C2RMF). She is developing spectral, 3D, and XR imaging in order to measure and understand artworks before restoration.

Jon Y. Hardeberg is Professor of Colour Imaging at NTNU, Department of Computer Science, The Norwegian Colour and Visual Computing Laboratory, Gjøvik, Norway. His current research interests include spectral imaging, image quality, colour management, material appearance, cultural heritage imaging, and medical imaging, and he has co-authored more than 300 publications within the field. He has led several research projects funded by the Research Council of Norway, been NTNU's representative in two Erasmus Mundus Joint Master Degrees (CIMET and COSI), and the coordinator of three Marie Sklodowska Curie ITN projects (CP7.0, ApPEARS, CHANGE).